Proceedings of the ECCOMAS Thematic International Conference on Simulation and Modeling of Biological Flows (SIMBIO 2011) September 21-23, 2011, VUB, Brussels, Belgium

Secondary Flows in Thoracic Aorta with Torsion

Hiroshi Suito[1,2], Takuya Ueda[3], and Daniel Sze[4]

1 Department of Environmental and Mathematical Sciences, Okayama University, 3-1-1, Tsushima-naka, Okayama, 700-8530, Japan, suito@ems.okayama-u.ac.jp

2 CREST, Japan Science and Technology Agency Kawaguchi, Saitama 332-0012, Japan

3 Department of Radiology, St. Luke's International Hospital, 9-1 Akashi-cho, Tokyo, 104-8560, Japan takuedarad@gmail.com

4 Department of Radiology, Stanford University, School of Medicine, Stanford, CA 94305, USA, dansze@stanford.edu

Abstract

Numerical simulations of blood flow in thoracic aorta and in simplified spiral pipes are presented. Patient-specific aorta shapes are used in a centerline-fitted generalized coordinate system in which the Navier–Stokes equation is discretized using finite-difference approximation with immersed boundary/fictitious domain method. The main target of this study is long-term adverse events that occur after endovascular stent–graft treatment. The occurrence of swirling flow in the diastole phase is investigated using simplified shapes of pipes with curvature and torsion.

Keywords: blood flow, numerical simulation, finite difference method, helical pipe.

Introduction

Thoracic endovascular aortic repair (TEVAR), or stent–graft treatment, has become widely accepted as an important option for treatment of thoracic aortic diseases. Many studies have proven the safety and efficacy of TEVAR with satisfactory short-term to mid-term outcomes. Nevertheless, even if the initial TEVAR treatment technically succeeds, some patients show recurrence and progression of disease many years after treatment[8][12]. Based on long-term follow-up examinations, such long-term morphological change and effects of hemodynamic flow apparently interact synergically. Constant pulsatile hemodynamic effects from blood flow apparently induce degeneration of the underlying aorta to cause its morphological change and to induce minor morphological changes that alter the hemodynamic state. These changes ultimately engender long-term adverse events.

For this study, which investigates the effect of vascular hemodynamics on long-term adverse events, we considered patient-specific models of the thoracic aorta—with and without aneurysms—as constructed from CT scans. The aorta is classifiable into a thoracic aorta and abdominal aorta, with several different characteristics. We specifically examine the thoracic aorta and the blood flow in it.

From the viewpoint of computational methods for blood flow simulations, there are mainly two discretization strategies: unstructured and structured meshes. When one is trying to compute flows using structured meshes, the important issue is how to represent the geometry in the structured mesh system. Many investigations of this problem have been done. Those efforts are broadly classifiable into two categories: a body-fitted approach and an immersed boundary or fictitious domain method [4][5]. An advantage of body-fitted mesh is its high accuracy near walls, although mesh generation near a complex-shaped boundary is often difficult. It can achieve high accuracy if one of its coordinate axes coincides with the main flow direction. In contrast, in the immersed boundary/fictitious domain method, mesh generation is simple because a uniform orthogonal mesh is useful and the wall geometry is represented by a distribution of a characteristic function. In this study, a hybrid approach between the body-fitted and immersed boundary/fictitious domain method is adopted as described in the next section. It can be expected that higher accuracy is attainable at reasonable computational cost using this hybrid approach. In the following sections, patient-specific simulations are presented followed by numerical tests using simplified geometry for investigating the effects of torsion.

Representation of aorta morphology

Procedures for the reconstruction of aorta morphology from medical images are the following:

i) Centerline and radius data from CT images

Median axis transform technique [6] is applied to extract the (x,y,z)-coordinate of the centerline and radius at position s from CT images, where s is a length along the centerline from the proximal end of aorta, as presented in Fig. 1.

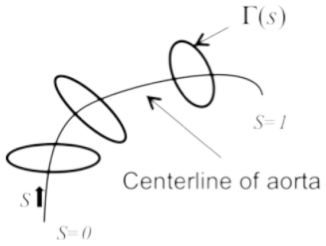

Fig. 1 Centerline and cross-sections.

ii) Generation of a centerline-fitted mesh

A finite difference mesh system (ξ,η,ζ) is generated, one coordinate axis of which is nearly parallel to the aorta centerline. Therefore, (ξ,η,ζ) is a generalized coordinate system, which represents the coordinate transformation from computational space (ξ,η,ζ) to physical space (x,y,z):

$$\begin{cases} x = x(\xi,\eta,\zeta) \\ y = y(\xi,\eta,\zeta) \\ z = z(\xi,\eta,\zeta) \end{cases}$$

The ζ- axis is set not to be strictly parallel but to be nearly parallel to the centerline, which means that the original centerline geometry is slightly smoothed by the Gaussian filter. This treatment avoids numerical instabilities arising from severe skewness of finite difference meshes.

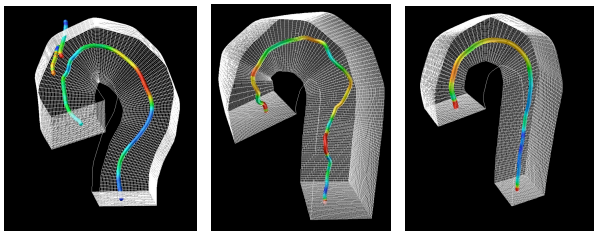

Fig. 2 Centerlines and finite-difference meshes.

Three examples of finite difference meshes are presented in Fig. 2 with the original centerlines extracted in the previous step. In this figure, only the planes at which ξ and η takes the minimum value and ζ takes the minimum and maximum values are shown. The centerline color represents curvature distributions.

iii) Generation of characteristic functions

On each mesh point defined in the previous step, the characteristic function is computed, which takes the value 0 in the aorta and value 1 out of the aorta. It varies gradually near the boundary with certain smoothness. The value of the characteristic function $\lambda(x,y,z)$ is computed as

$$\lambda(x,y,z) = \frac{1}{2}\left(1 + \tanh\left(\frac{r - r_0}{\varepsilon}\right)\right),$$

where $r(x,y,z)$ is a distance between the point (x,y,z) and the nearest point P_0 on the centerline, r_0 is a radius of the aorta at P_0, and ε is a smoothness parameter on the boundary. Figure 3 shows contour surfaces of the characteristic functions $\lambda(x,y,z)$ at $\lambda = 0.5$ with finite difference meshes constructed in the prior step.

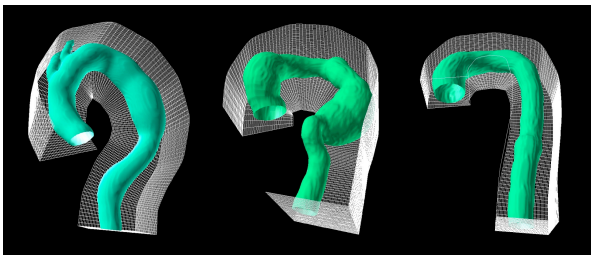

Fig. 3 Contour surfaces of characteristic functions.

Numerical methods

As governing equations, incompressible Navier–Stokes equations are used with the continuity equation

$$\begin{cases} \dfrac{\partial \boldsymbol{u}}{\partial t} + (\boldsymbol{u}\cdot\nabla)\boldsymbol{u} = -\dfrac{1}{\rho}\nabla p + \nu\nabla^2\boldsymbol{u} - \dfrac{1}{\varepsilon_f}\lambda\boldsymbol{u} \\ \nabla\cdot\boldsymbol{u} = 0 \end{cases}$$

where $\boldsymbol{u}$, p, t, ρ and $\nu = \mu/\rho$ respectively denote velocity, pressure, time, density and kinematic viscosity. The last term of the Navier–Stokes equations is a drag force term that is proportional to the fluid velocity because of the immersed boundary method. Because this force acts only out of the aorta, the flow velocity out of the aorta becomes zero and the aorta wall shape is represented. Drag force parameter ε_f is taken as $\varepsilon_f \approx \Delta t$, where Δt is a time step. Blood is assumed to be a Newtonian fluid because we are considering a flow in large vessels. The governing equations are discretized on the finite difference mesh and SMAC method is applied for time advances in which a Poisson equation for the increment of pressure field is solved to satisfy the conservation of mass. The Generalized Product type Bi-Conjugate Gradient method is adopted for solving the Poisson equation. At the proximal end, a pulsating velocity profile is given.

Numerical results

After computing the time dependent flow fields, we compute the time-averaged flow field and wall stresses from them. It is apparent that the stress distributions are

strongly dependent to the aorta morphology. Several reasons why such a large difference occurs can be considered. One possibility is the existence of swirling flow during the diastole phase, as portrayed in Fig. 4.

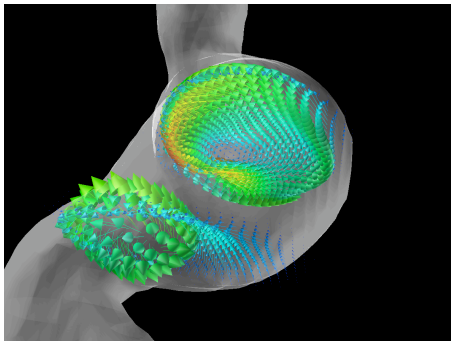

Fig. 4 Swirling flow in diastole phase.

Generally speaking, flow is almost annihilated in the diastole phase. Therefore, the existence of this swirling flow can be a key point in finding the critical parameter for the difference in stress distributions among individuals.

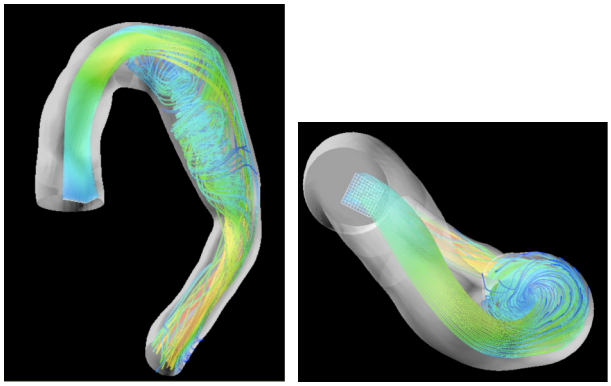

Side view Top view

Fig. 5 Instantaneous streamlines in late systole phase.

Fig. 5 shows instantaneous streamlines in late systole phase. It can be seen that a swirling flow appears immediately downstream of the tortuous part of the vessel.

Numerical tests in simplified geometry

From comparison of the flow fields of several examples of thoracic aorta morphologies presented in the previous section, it has been inferred that torsions of the centerline are a candidate of the critical parameter of the existence of swirling flow in diastole phases. Torsion is defined as a variation of the curvature in the following Frenet–Serret formula:

$$\frac{d}{ds}\begin{pmatrix}\boldsymbol{t}\\ \boldsymbol{n}\\ \boldsymbol{b}\end{pmatrix}=\begin{pmatrix}0 & \chi & 0\\ -\chi & 0 & \tau\\ 0 & -\tau & 0\end{pmatrix}\begin{pmatrix}\boldsymbol{t}\\ \boldsymbol{n}\\ \boldsymbol{b}\end{pmatrix},$$

where t denotes tangential, n denotes normal, and b denotes bi-normal vectors, respectively. In addition, χ and τ respectively signify the curvature and torsion. Normal vector n is directed to the center of the curvature. If the normal vectors near point s are on the same plane, then the torsion at s is zero. We use simple spirals defined as

$$\begin{cases}x = a\cos s\\ y = a\sin s\\ z = hs\end{cases}$$

for which the tangential, normal, and bi-normal vectors become

$$\boldsymbol{t}=\left(-\frac{a\sin s}{\sqrt{a^2+h^2}},\ \frac{a\cos s}{\sqrt{a^2+h^2}},\ \frac{h}{\sqrt{a^2+h^2}}\right)$$
$$\boldsymbol{n}=\left(-\cos s,\ -\sin s,\ 0\right)$$
$$\boldsymbol{b}=\left(\frac{h\sin s}{\sqrt{a^2+h^2}},\ -\frac{h\cos s}{\sqrt{a^2+h^2}},\ \frac{a}{\sqrt{a^2+h^2}}\right)$$

and the curvature and torsion are calculated as

$$\chi=\frac{a}{a^2+h^2},\quad \tau=\frac{h}{a^2+h^2}.$$

In those equations, a and h are arbitrary parameters. Figure 6 portrays four spirals with the sets of χ and τ.

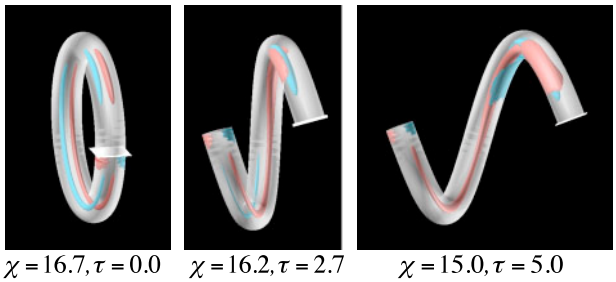

$\chi=16.7,\tau=0.0$ $\chi=16.2,\tau=2.7$ $\chi=15.0,\tau=5.0$

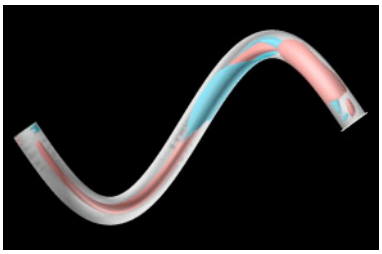

$\chi=11.5,\tau=7.7$

Fig. 6 Simple spiral tubes.

Secondary flow is computed by subtracting the axial flow $\boldsymbol{u}_{\text{axis}}$ from the total flow $\boldsymbol{u}$, as

$$\boldsymbol{u}_{\text{axis}}=(\boldsymbol{u}\cdot\boldsymbol{t})\boldsymbol{t}$$
$$\boldsymbol{u}_{\text{secondary}}=\boldsymbol{u}-\boldsymbol{u}_{\text{axis}},$$

which plays an important role in terms of wall stresses. Figure 7 and Fig. 8 respectively show secondary flow patterns in the two cases of τ =5.0 and τ =0.0.

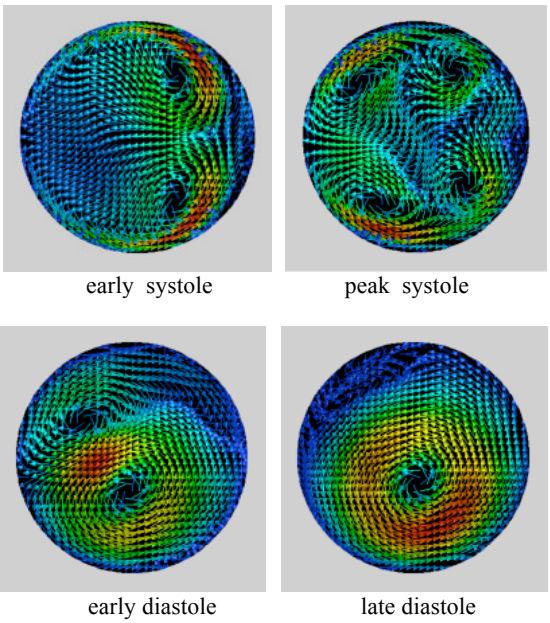

Fig. 7 Time-sequence of secondary flow for τ =5.0.

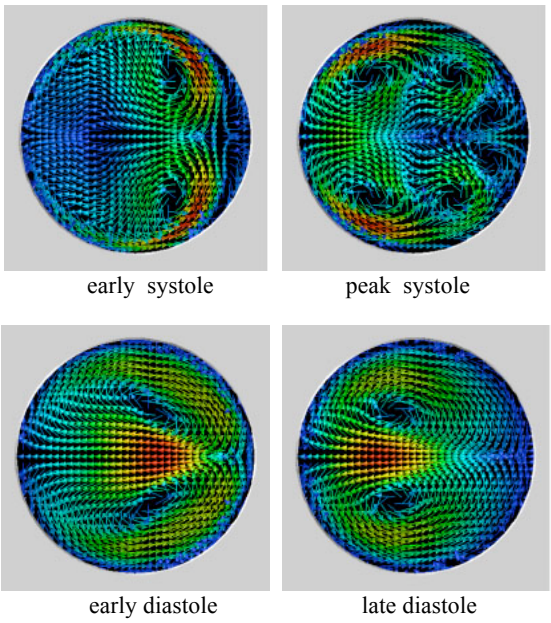

Fig. 8 Time-sequence of secondary flow for τ =0.0.

In both cases, twin vortices of opposite signs are visible in the early systole phase. These vortices are called Dean's vortices, which are common phenomena for flows in curved tubes. The center of the curvature exists on the right-hand-side of each figure. The centrifugal force is acting in the left-hand direction. In the peak systole phase, the Dean's vortices are split into smaller vortices in both cases.

However, the flow patterns in the diastole phase differ completely for the two cases. In the zero-torsion case, secondary flow maintains symmetry, which means that the torque exerted on the wall is zero. However, in the non-zero torsion case, the vortices generated in the systole phase merges and one grows larger. In the late diastole phase, only one vortex survives. Therefore, a certain amount of the torque is exerted on the wall, which has the effect of making the torsion larger.

Conclusions

Through computations of the flows in realistic aorta morphologies and in simplified spiral tubes, the importance of the torsion of aorta has been shown. All patients have certain curvature in their thoracic aorta because it projects upward from the heart and then arches downward. However the values of torsion can vary widely among patients. Results described herein suggest that the torsion is a more important parameter in considering the relation between aorta morphologies and the hemodynamics in them.

Acknowledgements

This work is supported by Japan Science and Technology Agency as a CREST project.

References

[1] C.Y. Wang, On the low-Reynolds-number flow in a helical pipe, *J. Fluid Mech*., **108**, pp. 185-194 (1981).

[2] M. Germano, On the effect of torsion on a helical pipe flow, *J. Fluid Mech*., **125**, pp. 1-8 (1982).

[3] S.A. Berger and L. Talbot, Flow in curved pipes, *Ann. Rev. Fluid Mech*., **15**, pp. 461-512 (1983).

[4] D. Goldstein, R. Handler, and L. Sirovich, Modeling a no-slip boundary with an external force field, *J. Comput. Phys*., **105**, pp. 354-366 (1993).

[5] H. Fujita, H. Kawahara, and H. Kawarada, Distribution theoretic approach to fictitious domain method for Neumann problems, *East–West J. Numer. Math.*, **3**, 2, pp. 111-126 (1995).

[6] G.D. Rubin, D.S. Paik, P.C. Johnson, and S. Napel, Measurement of the aorta and its branches with helical CT, *Radiology*, **206**, pp. 823-829 (1998).

[7] C.A. Taylor, T.J.R. Hughes, and C.K. Zarins, Finite element modeling of blood flow in arteries, *Comput. Methods Appl. Mech. Engrg.*, **158**, pp. 155-196 (1998).

[8] M. Tillich, R.E. Bell, D.S. Paik, D. Fleischmann, M.C. Sofilos, L.J. Logan, and G.D. Rubin, Iliac arterial injuries after endovascular repair of abdominal aortic aneurysms: correlation with iliac

curvature and diameter, *Radiology*, **219**, pp. 129-136 (2001).

[9] I.E. Vignon-Clementel, C.A. Figueroa, K.J. Jansen, and C.A. Taylor, Outflow boundary conditions for finite element modeling of blood flow and pressure in arteries, *Comp. Methods Appl. Mech. Eng.*, **195**, pp. 3776-3796 (2006).

[10] C.A. Figueroa, I.E. Vignon-Clementel, K.E. Jansen, T.J.R Hughes, and C.A. Taylor, A coupled momentum method for modeling blood flow in three-dimensional deformable arteries, *Comput. Methods Appl. Mech. Engrg*., **195**, pp. 5685-5706 (2006).

[11] K.E. Lee, K.H. Parker, C.G. Caro, and S.J. Sherwin, The spectral/hp element modeling of steady flow in non-planar double bends, *Int. J. Num. Meth. Fluids*, **57**, pp. 519-529 (2008).

[12] T. Ueda, D. Fleischmann, G.D. Rubin, M.D. Dake, and D.Y. Sze, Imaging of the thoracic aorta before and after stent-graft repair of aneurysms and dissections, *Semin. Thorac. Cardiovasc. Surg.*, **20**, 4, pp. 348-357 (2008).

[13] J.D. Humphrey and C.A. Taylor, Intracranial and abdominal aortic aneurysms: similarities, differences, and need for a new class of computational models, *Ann. Rev. Biomed. Eng*., **10**, pp. 221-246 (2008).

[14] H. Suito, T. Ueda, and G.D. Rubin, Simulation of blood flow in thoracic aorta for prediction of long-term adverse events, *Proceedings of the 1st International Conference on Mathematical and Computational Biomedical Engineering*, pp. 27-30 (2009).

[15] H. Suito, T. Ueda, M. Murakami, and G.D. Rubin, Vortex dynamics in thoracic aortic aneurysms, ECCOMAS CFD 2010, Laboratorio Nacional de Engenharia Civil, Lisbon, Portugal (2010).